ARTICLES

Multiple-scattering calculations of the uranium L_3-edge x-ray-absorption near-edge structure

E. A. Hudson
Glenn T. Seaborg Institute for Transactinium Science, Lawrence Livermore National Laboratory, University of California, Livermore, California 94551

J. J. Rehr
Department of Physics, University of Washington, Seattle, Washington 98195

J. J. Bucher
Chemical Sciences Division, Lawrence Berkeley National Laboratory, Berkeley, California 94720
(Received 5 June 1995; revised manuscript received 27 July 1995)

A theoretical study of the uranium L_3-edge x-ray absorption near-edge structure (XANES) is presented for several uranium compounds, including oxides, intermetallics, uranyl fluoride, and α-uranium. Calculations were performed using FEFF6, an *ab initio* multiple-scattering (MS) code that includes the most important features of current theories. The results, which account for both the fine structure χ and the atomiclike background μ_0 of the absorption coefficient μ, are compared to new and previously measured experimental spectra, reavealing very good agreement for most systems. For several compounds, a more detailed theoretical analysis determined the influence of cluster size and scattering order upon the calculated spectra. Results indicate that MS paths and scattering paths that include rather distant atoms make significant contributions for UO_2, whereas XANES for crystals with lower symmetry and density can be modeled using only shorter single-scattering paths. In most cases, assumption of a screened final state in the calculation gives better agreement with experiment than use of an unscreened final state. The successful modeling of spectra for a variety of different uranium compounds, with differing spectral features, indicates that the semirelativistic treatment of XANES used here is adequate even for heavy elements. The well-known resonance, observed experimentally for uranyl (UO_2^{2+}) compounds ≈ 15 eV above the white line, is successfully modeled here for the first time, using multiple-scattering paths within the O-U-O axial bonds. Overlapping muffin-tin spheres were required in the calculation, probably as a result of the short uranyl axial bonds.

I. INTRODUCTION

X-ray-absorption spectroscopy probes the local electronic and geometric structure around an atom of a selected chemical element. X-ray-absorption spectra can be divided into two regions which contain roughly complementary information: (1) extended x-ray-absorption fine structure (EXAFS) provides bond lengths, coordination numbers, and elemental identities for the first few coordination shells around an absorbing atom. (2) X-ray-absorption near-edge structure (XANES) reflects the oxidation state and local structure around the absorbing atom. Both approaches are element specific due to the characteristic binding energies of core electrons, and can be applied to disordered systems due to the limited volume around the absorbing atom which contributes to the fine structure. Because EXAFS arises from photoelectron-atom scattering and is well understood theoretically, it has become a widely used and accepted experimental technique.[1,2] The origin of XANES is more complex, and depends on a number of effects which are as yet not completely characterized. However, XANES is growing in popularity because it can provide unique information about chemical state, band structure, bond angles, and local structural order in a broad range of materials.[1,2]

In recent years, advances in theory have led to semiquantitative predictions of XANES for a variety of systems. The starting point for these models is the EXAFS effect,[3] whereby the photoelectron wave produced by x-ray excitation scatters off neighboring atoms and is partially reflected back to the emitter atom, where it interferes with the outgoing wave and modulates the x-ray-absorption cross section. In the EXAFS regime, this effect is dominated by simple backscattering paths from nearby atoms. For XANES, the mean free path of the photoelectron can be much larger and the probability of off-linear scattering increases. Both of these differences tend to increase the number of scattering paths which contribute significantly to the x-ray-absorption cross section. In particular higher-order scattering, i.e., multilegged paths involving several atoms, becomes more important. Essential features of successful scattering formulations for XANES include the consideration of

multiple-scattering paths,[4,5] use of a complex energy-dependent self-energy,[6,7] and, for systems with high-Z atoms, at least, semirelativistic scattering potentials.[8,9] Relativistic effects on the scattering states themselves are small, but perhaps not negligible.[8] In some cases, a one-electron approach is not entirely adequate, and consideration of multielectron excitations must also be included.[7,10,11]

In this paper, we present a theoretical study of uranium L_3-edge XANES for several uranium compounds, including oxides and intermetallics. The electronic structure of uranium, and the f elements in general, has been a topic of considerable interest for many years.[12] Attention has focused, in part, on the relationship between band structure and unusual magnetic and superconducting properties. Uranium is of particular interest because it exhibits intermediate localization of the f electrons. Uranium XANES, using d initial states, has been used to probe this important property directly.[13–15] Due to dipole selection rules, XANES at the L_3 edge, with the $2p_{3/2}$ initial state, accesses the unoccupied d band. Localization issues are also important for these states.[13,15,16] Other investigations of actinides with x-ray-absorption spectroscopy focus on the determination of structure and speciation for actinides in solution[17–19] or in geological systems,[20–23] motivated mainly by environmental concerns. The current work provides theoretical tools for the interpretation of XANES in a broad range of actinide research.

Calculations were performed using FEFF6,[24–26] a general-purpose x-ray-absorption spectroscopy code which includes all the features described above except multielectron excitations and relativistic scattering states. Results of simulations are compared to new and previously measured experimental spectra, revealing very good agreement for a number of systems. For several compounds, a more detailed theoretical analysis determined the influence of cluster size and scattering order upon the calculated spectra. Results indicate that third-order multiple-scattering paths, as well as first- and second-order scattering paths to rather distant atoms, make significant contributions for uranium dioxide, whereas XANES for crystals with lower symmetry and density can be modeled using only shorter single-scattering paths. Calculations which assume either a screened or an unscreened core hole are compared. Overall, use of a screened final state gives better agreement with experiment. However, for uranium dioxide, an unscreened final state produces a better model of the white line intensity. FEFF6 uses a combination of fully relativistic atomic potentials, semirelativistic scattering phase shifts, and a nonrelativistic multiple-scattering expansion with the usual l,m angular momentum basis. The successful modeling of spectra for a variety of different uranium compounds, with differing spectral features, indicates that this semirelativistic treatment of XANES is adequate even for heavy elements.

The above-edge resonance which is observed experimentally for uranyl fluoride and other uranyl compounds has been attributed to either a shake-up process[27] or a localized multiple-scattering resonance.[13,14] Until now there has been no direct theoretical consideration of either explanation. This resonance is successfully modeled here for the first time, using multiple-scattering paths with the O—U—O axial bonds. Overlapping muffin-tin spheres were required in the calculation for this system, probably as a result of the short uranyl axial bonds.

We are aware of only two previous theoretical studies of actinide XANES. Guo *et al.* presented multiple-scattering XANES calculations for the uranium M edges in crystalline UO_2 and molecular UCl_4.[9] Results were in good agreement with experimental measurements. In a paper by Tyson, relativistic and nonrelativistic calculations of electron-scattering parameters were compared for the Th L_2 and L_3 edges.[8] The present work represents the first comparison of calculated actinide L_3-edge XANES to experimental results.

II. THEORETICAL APPROACH AND COMPUTATIONAL DETAILS

FEFF was originally developed as a theoretical EXAFS standard, allowing the calculation of reliable scattering phase shifts and amplitudes for use in fitting experimental EXAFS. The basic theoretical formulation has been described in some detail.[25,26] In short, it performs an *ab initio* curved-wave single-scattering calculation within a muffin-tin potential, using a complex energy-dependent self-energy to model exchange-correlation effects and inelastic losses. FEFF5 introduced a separable Green's-function formulation for higher-order scattering, and an efficient sorting scheme to handle the potentially large numbers of multiple-scattering paths.[5,28] These improvements, among others, facilitated the accurate calculation of XANES, and in fact FEFF5 was successfully used to model experimental results.[5,29,30] However, because of its roots in EXAFS, the code calculated only the oscillatory x-ray-absorption fine structure χ as a function of k, the photoelectron momentum.

In the most recent version, FEFF6, additional calculations have been included to allow the determination of $\mu(E)$, the absorption coefficient, as a function of the x-ray energy E.[24,31] One of the formal difficulties associated with a complex self-energy is that $\mu_0(E)$, the atomiclike absorption background, does not factor out from the fine structure.[32] But by neglecting the small contribution to $\mu_0(E)$ from the imaginary portion of the irregular (i.e., singular at the origin) part of the final-state wave function [$R_L^+(\mathbf{r})$ in Ref. 32, which vanishes for real potentials], the expression for $\mu(E)$ factors into a form analogous to that for real potentials, $\mu(E)=\mu_0(1+\chi)$.[31] Using a well-defined absolute threshold energy E_0, the fine structure χ can be expressed as a function of E, where $[E-E_0]\propto k^2$.

For a given initial state nl, $\mu_0(E)$ is calculated using the $(l+1)_{l+1/2}$ final state, which is derived for the scattering calculations, and the core atomic orbitals available from the construction of the scattering potential.[24,31] These atomic wave functions are determined using the self-consistent, relativistic, Dirac-Fock-Slater atom code of Desclaux.[33] Semirelativistic scattering phase shifts are determined from these relativistic atomic potentials by

matching the Dirac equation solution at the muffin tin radius, using a method of Loucks.[34] Scattering is otherwise treated nonrelativistically, using a multiple-scattering expansion with the usual l,m angular momentum basis. Thus the determination of $\mu_0(E)$ is almost fully relativistic, while that of $\chi(k)$ is only semirelativistic.

Muffin-tin potentials are good models for metals, but may be less reliable for structures with strong directional bonding. In cases of severe anisotropy, the nonoverlapped muffin-tin spheres used by default in FEFF6 may lead to large discontinuities in the derived potential at the edges of muffin-tin spheres. This problem may be avoided by using overlapped muffin-tin spheres, which removes self-consistency from the potential, but nevertheless may lead to better agreement with experiment, as demonstrated below for UO_2F_2.

The EXAFS spectrum $\chi(k)$ is a coherent sum of oscillatory contributions from each individual scattering path. Thus a limited number of scattering paths can be used to approximate XANES, because the multitude of paths which make very weak contributions to $\chi(k)$ will tend to cancel each other.[28] FEFF5 and FEFF6 have several strategies to filter out the unimportant paths efficiently, as described in Ref. 24. For all the XANES simulations presented here, convergence was ensured by including additional paths beyond the final path set, and verifying that they did not alter results. Once the path set required for convergence is determined, it may be instructive to remove some paths by decreasing the limits on cluster size, path length, and scattering order. By following the changes in the calculated spectrum as the path set is reduced, one can sometimes identify the origin of specific spectral features in a subset of scattering paths. For several of the compounds modeled here, such a path analysis is presented to demonstrate the relative importance of various types of paths. For all calculations, atomic clusters of radius ≈ 7 Å were used, even when scattering paths were restricted to a much smaller volume. This cluster size ensured a converged scattering potential for all the atoms involved in significant scattering paths.

One of the primary reasons for the larger numbers of scattering paths required for the modeling of XANES, in comparison to EXAFS, is the increased mean free path (MFP) of the photoelectron at low kinetic energy (i.e., <30 eV). Recent FEFF5 calculations of XANES for alkali halides demonstrated the importance of rather long scattering paths.[29] For example, the Na K-edge XANES of NaBr was best modeled by including paths up to 26 Å long (i.e., up to a cluster radius of 13 Å). In the case of uranium L_3 XANES, however, the *effective* mean free path of the photoelectron is severely constrained by the short lifetime of the $2p_{3/2}$ core hole. The uranium $2p_{3/2}$ core hole has a natural linewidth of 7.4 eV,[35] which effectively limits the MFP to <6 Å for kinetic energies in the XANES region. Based on this limitation, one may predict that uranium L_3 XANES calculations should converge using a fairly small set of scattering paths, and indeed this result was obtained in the present calculations. In fact, the effective MFP is actually *larger* in the higher EXAFS region than in the XANES region, contrary to the trend normally observed.

The current FEFF6 code uses an approximate treatment of core-hole lifetime, which separately broadens $\mu_0(E)$ and $\chi(E)$. For the present calculations, a more accurate approach was used, which explicitly broadens the final result $\mu(E)$. This improvement resulted in significantly better agreement with experiment for line shapes, widths,

TABLE I. Structural details of uranium compounds. Interatomic distances (R) and coordination numbers (N), relative to a central uranium atom, are listed for the first coordination shell and for the first coordination shell containing uranium. Both total and uranium-only atomic number densities are also shown. References are listed for the crystal structures used in the calculations.

Compound	Crystal structure	Atom number density: total, uranium ($10^2 \times n$ Å^{-3})	First shell: R (Å), N	First uranium shell: R (Å), N
UO_2	cubic (CaF_2)[a]	7.3, 2.4	2.37, 8	3.87, 12
U_3O_8	orthorhombic[b,c]	6.6, 1.8	2.07, 2	3.76, 2
			2.07, 2	3.76, 1
UO_2F_2	rhombohedral[d]	6.3, 1.3	1.74, 2	4.19, 6
α-uranium	orthorhombic[a]	4.8, 4.8		2.75, 2
UNi_5	cubic ($AuBe_5$)[e]	7.7, 1.3	2.81, 12	4.80, 12
UCu_5	cubic ($AuBe_5$)[e]	6.9, 1.1	2.92, 12	4.97, 12
UIn_3	cubic ($AuCu_3$)[f]	4.1, 1.0	3.25, 12	4.60, 6
UAl_2	cubic ($MgCu_2$)[f]	5.1, 1.7	3.22, 12	3.36, 4
UMn_2	cubic ($MgCu_2$)[f]	6.5, 2.2	2.97, 12	3.10, 4
UAs	cubic (NaCl)[a]	4.2, 2.1	2.88, 6	4.08, 12
USb	cubic (NaCl)[a]	3.4, 1.7	3.10, 6	4.38, 12

[a]Reference 46.
[b]Two distinct uranium sites.
[c]Reference 47.
[d]Reference 48.
[e]Reference 49.
[f]Reference 50.

and intensities in the edge-jump and white-line regions.

For many of the compounds modeled here, Debye temperatures are not available and therefore Debye-Waller (DW) factors were assumed to be zero, i.e., the dampening effects of disorder were not considered. This approximation tends to overestimate the relative contributions from (a) scattering paths through lighter atoms, which have more extended spatial distributions due to the mass dependency of thermal motion; and (b) higher-order multiple-scattering (MS) paths, which are dampened by the disorder of several atoms. The Debye temperature for uranium dioxide is known;[36] a simulation is presented below which includes the treatment of thermal disorder by the correlated Debye model.[37]

Upon creation of a core hole by absorption of an x ray, there is often a rearrangement of local electronic structure to screen the positive charge of the hole. In fact, x-ray photoelectron spectroscopy has shown that distinct screened and unscreened core-ionized final states are possible for a variety of systems.[38–41] In FEFF a screened final state is modeled simply by including an extra electron in the lowest unoccupied orbital of the core-excited atom before calculating the muffin-tin potential. Calculations based on both screened and unscreened final states are compared in this paper. Overall, the screened final state gives better agreement with experiment, but there are some exceptions described below. Work is in progress to develop theory and code to treat the possibility of multiple final states in a unified way.

To calculate XANES, FEFF6 requires as input parameters the positions of all atoms within the chosen cluster. Therefore all the simulations presented in this paper are based on structural information from the published literature, summarized in Table I. Ultimately it is desirable to model experimental XANES using FEFF6 for systems where detailed structural information is unavailable. This may be possible in some cases, especially where direct comparisons to spectra of related known structures are possible. The situation is similar for EXAFS, where the technique is most successful when applied to unknown systems for which there is already some idea of the possible structures. In fact, the results presented in this paper establish a basis for the modeling of actinide L_3 XANES spectra in systems which are not fully characterized. In particular, results show that the uranium L_3 XANES for a variety of intermetallic compounds can be modeled with relatively small clusters and without MS. Therefore modeling of XANES for related unknown systems may be possible using a fairly small set of adjustable structural and nonstructural parameters.

III. RESULTS

A. Experimental data

To test the accuracy of the theoretical approach, calculated spectra are compared to new experimental spectra and to previously published measurements. U L_3-edge spectra of UO_2 and U_3O_8 were measured in transmission mode on the wiggler beamline 4-1 at the Stanford Synchrotron Radiation Laboratory. An estimated spectral resolution of ≈ 5 eV was obtained from the double-

TABLE II. Comparison of derived parameters from experimental and calculated spectra. To ensure the most consistent comparison, the experimental energies reflect a recalibration of absolute energy scale, as indicated. The parameters, defined in the text, characterize the edge jump and white-line (WL) region of the XANES. WL intensity is given in units of eV x (normalized absorption). References are listed for the experimental spectra, along with the energy shifts used for recalibration.

Compound	Experiment			Calculated (screened)			Calculated (unscreened)		
	Edge energy (keV)	WL half-width (eV)	WL intensity	Edge energy (keV)	WL half-width (eV)	WL intensity	Edge energy (keV)	WL half-width (eV)	WL intensity
UAs[a]	17.1632	11.56	26.22	17.1476	7.86	24.47	17.1422	6.52	24.89
USb[a]	17.1636	10.71	25.79	17.1476	7.81	24.68	17.1424	6.40	24.43
UCu_5[b]	17.1621	11.16	25.26	17.1480	9.97	24.38	17.1431	7.57	23.66
UNi_5[b]	17.1627	13.01	24.60	17.1464	11.85	23.68	17.1417	11.14	23.92
α-U[b]	17.1619	11.88	23.44	17.1427	11.19	22.63	17.1374	9.68	23.73
α-U[c,d]	17.1607	13.18	22.11						
UMn_2[c]	17.1613	13.62	23.32	17.1451	10.54	23.23	17.1396	8.77	23.93
UAl_2[c]	17.1618	11.16	24.34	17.1456	9.33	24.20	17.1405	7.65	23.95
UIn_3[c]	17.1603	10.57	24.42	17.1467	7.63	24.39	17.1429	6.48	21.87
UO_2[e]	17.1640	7.47	27.10	17.1484	7.35	25.23	17.1425	6.07	26.56
U_3O_8[e]	17.1663	10.2	25.94	17.1493	10.47	25.54	17.1444	7.82	26.50
UO_2F_2[f]	17.1658	8.52	25.54	17.1499	16.33	24.18	17.1447	6.54	26.47

[a]Reference 16; $\Delta E = +4.5$ eV.
[b]Reference 13; $\Delta E = +0.0$ eV.
[c]Reference 15; $\Delta E = +5.8$ eV.
[d]Experimental α-U XANES data set used in Fig. 3.
[e]This work: $\Delta E = +4.1$ eV.
[f]Reference 42; $\Delta E = +8.0$ eV.

crystal monochromator with Si(220) crystals, detuned 50% to reject higher-energy harmonics. The UO_2 (99.9% purity) was a -200 mesh powder (Noah Chemical, Farmingdale, NY). The U_3O_8 (99.8% purity) was a -100 mesh powder (Cerac, Milwaukee, WI). These chemicals were mixed with a powdered boron nitride buffer to give 3-mm-thick samples with an L_3 absorption edge jump of ≈ 1.7 and ≈ 1.0 for UO_2 and U_3O_8, respectively.

Measured U L_3 XANES from several publications are also reproduced here. Kalkowski *et al.* published spectra for several oxides and intermetallics, as part of a broad survey of actinide XANES at many edges and for many compounds.[13] Spectra for UAs and USb were taken from another paper by Kalkowski *et al.*, which compared XANES for uranium, plutonium, and neptunium compounds.[16] Lawrence *et al.* measured spectra for a series of uranium intermetallics in the context of a study of XANES white-line characteristics for uranium and rare-earth compounds.[15] The spectrum for α-U used in Fig. 3 is from this source. An unpublished UO_2F_2 spectrum from the same experimental run is also presented here.[42] For the comparison, the absolute photon energy scales of spectra from differing sources have been adjusted to give the most consistent relative calibration possible (see Table II). The energy scales used in all the plots are those produced by the calculations. In general, these tend to be $\approx 15-20$ eV lower than experiment; however, they provide a uniform reference for comparisons to experimental results from a variety of sources. The recalibrated energy scales of the individual experimental spectra have been shifted to facilitate the comparisons, as listed in the figure captions. For the comparison, the x-ray-absorption coefficient in each experimental spectrum has been normalized to equal unity at a photon energy ≈ 80 eV above the edge jump, and zero below the edge jump. This method of scaling is not ideal, and allowance for possible small variations should be made in the comparisons to calculations. To account for instrumental broadening, all calculated spectra have been convoluted with a Gaussian function of 5-eV full width at half maximum (FWHM).

B. Comparison of calculated and experimental XANES

Figures 1–3 show a comparison of calculated and experimental uranium L_3 XANES. Results of calculations assuming a screened or unscreened core hole in the final state are plotted. Overall, the agreement with experimental XANES is quite good, especially using the screened final state. In nearly every case, the calculations are successful in reproducing the relative energies, widths, and intensities of all the experimental fine-structure features. The notable exception is UO_2F_2, which is discussed below. Even the white lines (i.e., the most intense resonance in each spectrum, just above the edge jump) are modeled reasonably well in most cases. Besides modeling features within individual spectra, the calculations also reproduce some trends between compounds. See, for example, the reduced white-line maximum, increased white-line asymmetry, and reduced fine-structure amplitude of UMn_2 vs UAl_2 (Fig. 2). Many features above the white line are too narrow and too intense in the calculated spectra. This may be a consequence of ignoring thermal broadening in the calculation. A separate calculation for UO_2, discussed below, included thermal broadening and obtained a closer match to experiment. For all calculated spectra, the fine structure arises principally from $\chi(k)$, as expected. Each calculated $\mu_0(E)$ (not shown) exhibits only an edge jump, a single resonance at slightly higher energy, and no other structure. The width and intensity of this white-line resonance in $\mu_0(E)$ varies somewhat between compounds. Note that, in general, the white line in $\mu(E)$ also includes a significant contribution from $\chi(k)$.

In order to quantify the comparison between experiment and calculations in the edge jump and white-line region, several parameters were extracted from both theoretical and measured spectra. These parameters, list-

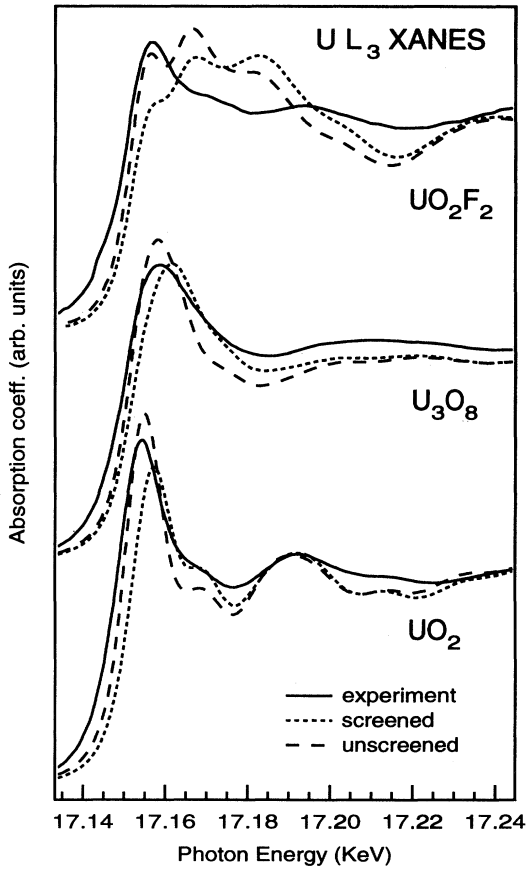

FIG. 1. Comparison of experimental and calculated uranium L_3-edge XANES for several oxygen-containing compounds. Results of calculations assuming a screened or an unscreened final state are plotted. All spectra calculated using the unscreened final state have been shifted $+4$ eV in energy to facilitate comparison. References for experimental spectra are given in Table II. For purposes of comparison, experimental photon energies have been shifted by -20 eV from the recalibrated energy scale used for Table II. A constant offset has been added to each curve, to separate spectra for the different compounds.

ed in Table II, are defined as follows: (A) edge energy—the energy corresponding to a normalized absorption of one-half; (B) white-line half-width—the difference between the energy of the point on the edge jump with half the maximum absorption and the energy of the first maximum; and (C) white-line intensity—the integral of the normalized absorption over an energy range -15 to $+20$ eV, relative to the edge energy. Note that trends in the experimental results are most reliable within sets of spectra taken from a single source.

Examination of the results in Table II reveals several interesting trends. The absolute edge energies are generally $\approx 15-20$ eV too low in the calculations; this $\approx 0.1\%$ accuracy is reasonable for the level of approximation used here. The experimental trends in *relative* edge energies are not completely reproduced by the calculations, although the results using a screened final state show agreement within ≈ 0.5 eV for USb, UAs, UMn_2, UAl_2, and UO_2. This level of success is, in fact, beyond expectations for the formulation used here, which was designed mainly for accurate modeling of electron scattering. The screened final state gives white-line half-widths which are somewhat smaller than the experimental values, but are closer than the half-widths from the unscreened final state. Experimental trends in half-widths are not well modeled, with the exception of UO_2 and U_3O_8, for which the screened final state reproduces the absolute and relative values quite well. The white-line intensity results do not clearly favor one of the final-state models. The relative intensities are reproduced, using the screened final state, for UNi_5, UCu_5, and α-U. Both relative and absolute intensities are reproduced, again using the screened final state, for UMn_2, UAl_2, and UIn_3. The unscreened final state, however, is a more successful model of the relative intensities for USb and UAs, and of the absolute intensity for UO_2. The observed experimental trends in the white-line widths and intensities can be related to the degree of localization of the unoccupied d band, as discussed in Refs. 13, 15, and 16. In fact, the ability of XANES to probe this property was the primary motivation for those experiments.

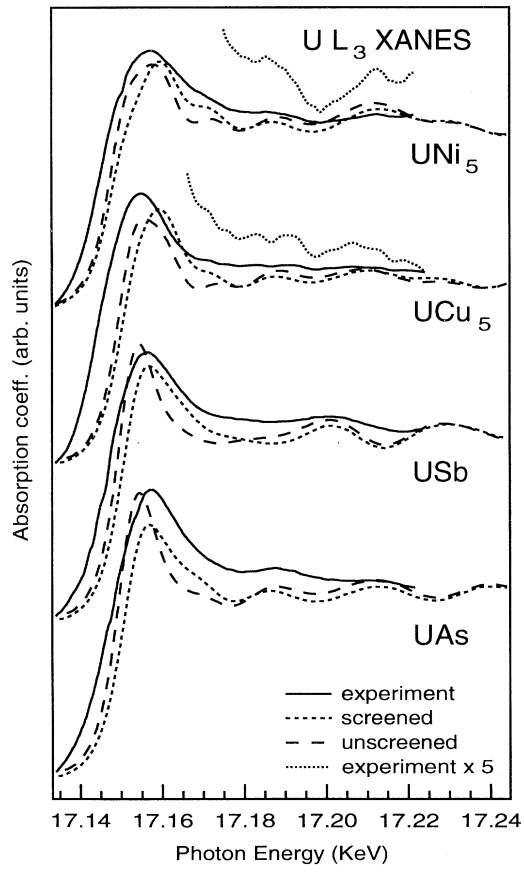

FIG. 2. Comparison of experimental and calculated uranium L_3-edge XANES for several uranium intermetallics. Expanded offset plots for two of the experimental spectra are also shown. See Fig. 1 for further details.

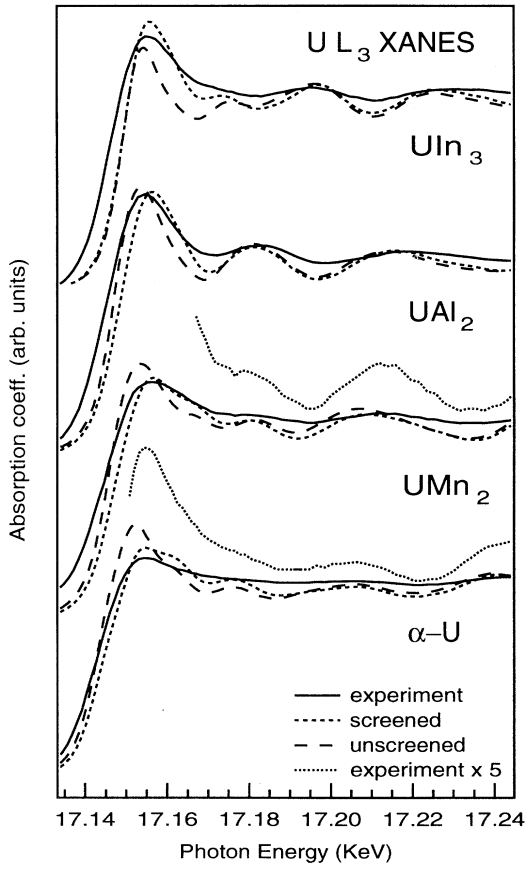

FIG. 3. Comparison of experimental and calculated uranium L_3-edge XANES for α-uranium and several uranium intermetallics. Expanded offset plots for two of the experimental spectra are also shown. See Fig. 1 for further details. To facilitate comparison, the photon energy of the UIn_3 experimental spectrum has been shifted by -17 eV (instead of the -20 eV used for the other experimental curves).

C. Scattering path analysis

1. Uranium dioxide

The Debye temperature of UO_2 has been experimentally determined to be 377 K.[36] Figure 4(a) compares calculations made using the correlated Debye model to the experimental room-temperature XANES. Note that, for both screened and unscreened final states, the above-edge features are broadened, giving a better agreement with experiment than for the comparison in Fig. 1, i.e., without the correlated Debye model. Shoulder *B* is better modeled by the screened final state. The white-line and edge-jump regions are unaffected by the thermal broadening; in fact the parameters derived from the calculated spectra are nearly identical to those listed for UO_2 in Table II.

Figures 4(b)–4(d) show the results of a scattering path analysis for UO_2. Each calculation employed the correlated Debye model, a screened final state, and the same electronic potential. The differences lie in the selection of scattering paths used to determine the fine structure. The fully converged (i.e., "full") calculation is reproduced as the solid line in each part of Fig. 4. Other curves show XANES calculated using subsets of the full path set. Figure 4(b) compares first-order (i.e., single-scattering or SS) calculations using one or two coordination shells. The single-shell result is clearly inadequate; however, the two-shell calculation roughly resembles the converged result, especially in the region of peak *C*. Figure 4(c) shows the results of using seven coordination shells, i.e., the full cluster, with first- and second-order scattering. Increasing the number of coordination shells from two to seven leads to a *poorer* SS result, but the subsequent addition of three-legged scattering paths (i.e., double scattering or DS) greatly improves the agreement with experiment [see Fig. 4(a)] in the region of shoulder *B* and peak *D*. Although the inclusion of DS also gives a slightly poorer agreement for peak *C*, this comparison provides clear evidence of the importance of MS paths in this spectrum. The fully converged result differs from the second-order result only by the inclusion of third-order scattering. The converged calculation gives a better agreement with experiment than the DS result, particularly for shoulder *B* and peak *C*. This indicates that third-order, i.e., four-legged, scattering paths make significant contributions to XANES.

The fully converged calculation for UO_2 used 58 inequivalent scattering paths (i.e., not counting degeneracies) within a seven-shell cluster. It is possible, however, to reduce the number of paths without significantly changing the result. Figure 4(d) shows XANES obtained using 24 carefully selected paths within a six-shell cluster. Indeed, the reduced path set gives a result which is very similar to the full calculation and agrees equally well with experiment. Figure 4(d) also shows the spectrum obtained when this reduced path set is modified by removing the three paths which involve sixth-shell atoms. The agreement with experiment for peak *D* is significantly worse when the smaller path set is used, as shown in the enlarged sections of the curves. This difference arises from scattering paths which include the sixth-shell atoms, not only in first order, but also in second order. The best agreement with experiment for peak *D* is only obtained when the calculation includes three-legged near-linear scattering paths to the sixth-shell uranium atoms. These two paths involve focusing either through second- or fourth-shell oxygen atoms, with a scattering angle of 29° in both cases (where 0° represents no deflection). The large influence of these paths arises in part from their large degeneracy—there are 48 ways to build each of these two paths.

2. Uranium intermetallics

Figure 5 shows the result of a path analysis for UAs. The situation here is much simpler than for UO_2. The re-

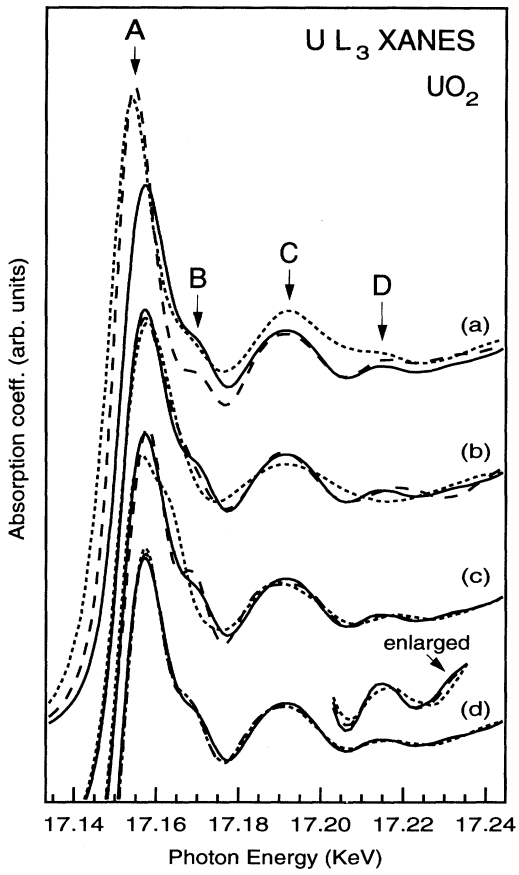

FIG. 4. The influence of different types of scattering paths upon the calculated UO_2 XANES. See text for details. (a) Solid–full calc. (screened, MS 7 shells); long dash—unscreened full calc. (shifted +4 eV); short dash–experiment (shifted −20 eV). (b) Solid—full calc.; short dash—SS one shell; long dash–SS two shells. (c) Solid–full calc.; short dash—SS seven shells; long dash—DS seven shells. (d) Solid–full calc.; short dash—reduced path set (five shells); long dashed—reduced path set (six shells). The curves in (d) are also plotted using an expanded offset absorption scale. The best agreement with experiment is obtained using multiple scattering and six coordination shells.

sult of the full calculation [Fig. 5(b)], with five coordination shells and multiple scattering, is duplicated using only two shells and single scattering [Fig. 5(d)]. Similar results were found for most other intermetallics.

UAl_2 exhibits somewhat more complicated behavior, as shown in Fig. 6. In this case, a SS calculation with six coordination shells [Fig. 6(d)] gives agreement with experiment that is comparable to that obtained for the six-shell MS calculation [Fig. 6(b)]. The MS result models the energy of peak *A* more closely, while the SS result better reproduces the relative intensity of shoulder *B*. The curve shown in Fig. 6(c) is obtained by adding only one MS path to the SS path set of Fig. 6(d). The result is nearly the same as the full MS curve [Fig. 6(b)], indicating that one MS path accounts for nearly all the difference between MS and SS. The MS path in question is a three-legged linear path to a sixth-shell uranium atom, focused by scattering through a first-shell aluminum atom. It is interesting to note that the best agreement with experiment would arise from a curve intermediate between those of Figs. 6(c) and 6(d), suggesting that the contribution of the MS path is somewhat overestimated by FEFF6. The SS result using only two coordination shells [Fig. 6(e)] is nearly converged, except for the absence of shoulder *B*. Path analysis results similar to those of UAl_2 were obtained for the related compound UMn_2 (not shown).

3. *α-uranium*

Figure 7 shows the result of a path analysis for α-U. The fine structure has very little amplitude in the experimentally measured XANES. However, that fine structure is roughly reproduced by the converged calculation [Fig. 7(b)], with an overestimated amplitude. Differences are observed in XANES as the scattering path set is reduced, first by eliminating MS [Fig. 7(c)], and then by decreasing the number of shells [Figs. 7(d) and 7(e)]. (Note that α-U has a rather asymmetric crystal structure, so the distance to the eighteenth shell is only ≈ 6.5 Å.) Comparison to the experimental XANES suggests that the calculation overestimates the influence of MS and distant scatterers; however, these conclusions are tentative due to noise in the experimental XANES.

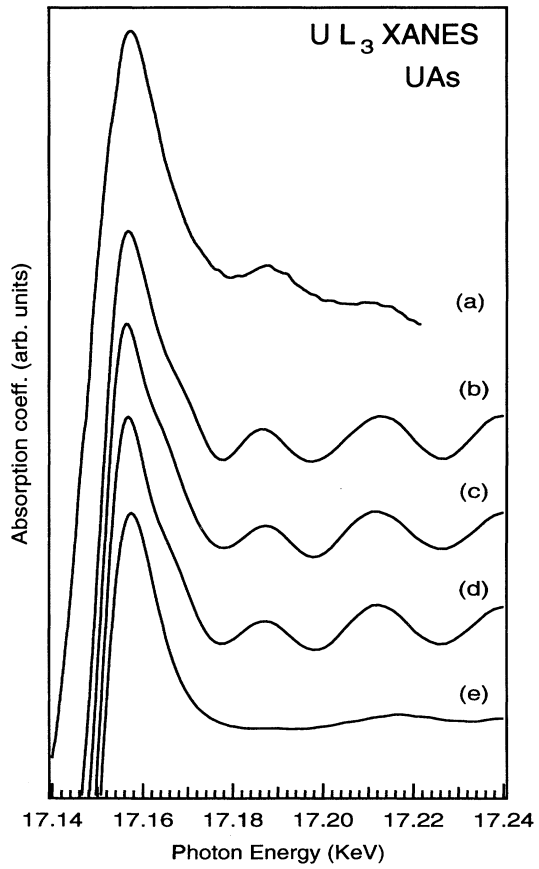

FIG. 5. The influence of different types of scattering paths upon the calculated UAs XANES. (a) Experiment (shifted −20 eV). (b) full calc. (MS five shells), (c) SS five shells, (d) SS two shells, (e) one SS shell. The calculation is nearly converged with only two coordination shells and single scattering.

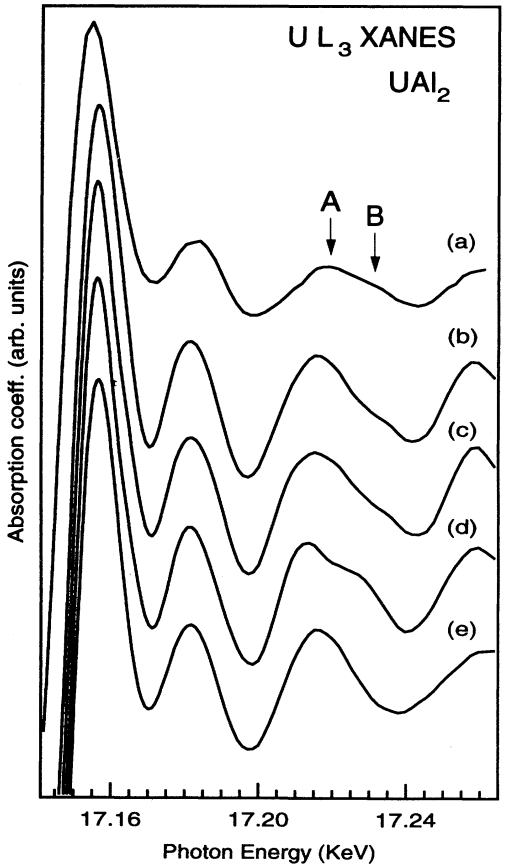

FIG. 6. The influence of different types of scattering paths upon the calculated UAl_2 XANES. (a) Experiment (shifted −20 eV), (b) full calc. (MS six shells), (c) SS six shells, plus one MS path, (d) SS six shells, (e) SS two shells. Six coordination shells are necessary to obtain the best agreement with experiment. Only one multiple-scattering path makes a significant contribution to the XANES.

4. *Uranyl fluoride*

The calculated XANES in Fig. 1 for UO_2F_2 shows very poor agreement with the experimental spectrum, possibly because the linear O-U-O uranyl group has unusually short bond distances between uranium and the axial oxygens (see Table I). Generally, modeling of such structural anisotropy may be improved in the calculation by overlapping the muffin-tin spheres of adjacent atoms. Figure 8 shows the results of calculations for UO_2F_2 using muffin-tin radii equal to the Norman radii (i.e., large overlap). The agreement with experiment is better in this case, especially when the screened final state is assumed. There is still some discrepancy in the energies of peak *B* and valley *C*, but the relative energies and intensities of the white line and peak *A* now match those of the experimental spectrum.

The full calculation in Fig. 8(a) used 57 scattering paths. However a calculation using only the 11 most important paths, shown in Fig. 8(b), gives a similar result. Figure 8(c) shows the result of further reducing the path set to include only paths within the first shell, i.e., three linear MS paths and one SS path. Although the white line is much less intense and the higher-energy features are missing, there is now a rather intense peak corresponding to shoulder *A*. This result strongly suggests that shoulder *A* arises primarily from scattering off the axial oxygens of the uranyl moiety. Two of these MS paths have a length three times that of the SS path. If those paths are removed, the curve in Fig. 8(d) results. This is now using only two paths—one SS and one MS. Peak *A* is a bit broader, but still intense. Figure 8(e) plots the result obtained using only the SS path. Peak *A* is missing, indicating that, in experimental XANES, shoulder *A* is a result of multiple scattering.

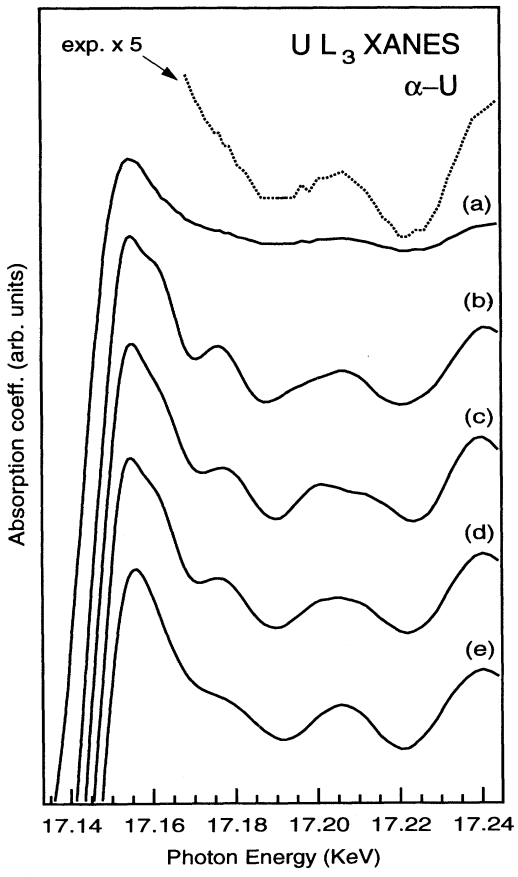

FIG. 7. The influence of different types of scattering paths upon the calculated α-U XANES. (a) Experiment (shifted −20 eV), including expanded, offset plot (dotted), (b) full calc. (MS 18 shells), (c) SS 18 shells, (d) SS ten shells, (e) SS five shells. Multiple scattering and scatterers beyond the tenth shell have a notable influence on the calculated XANES.

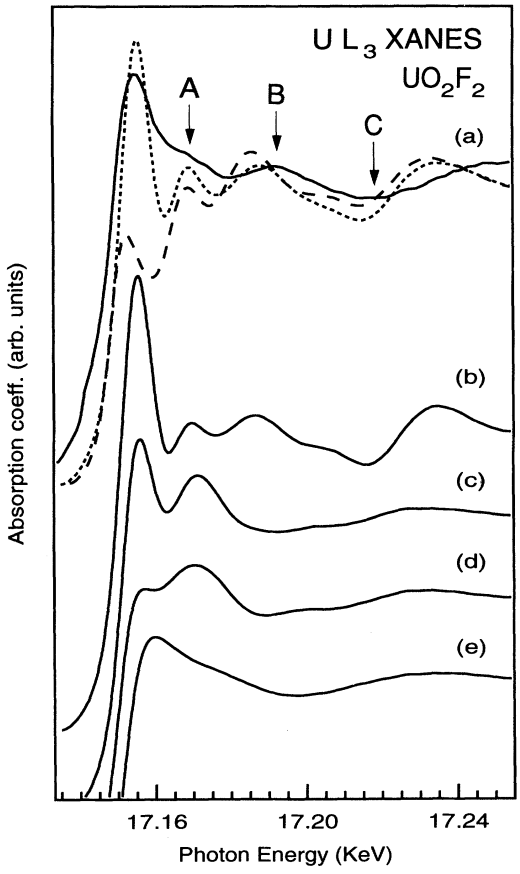

FIG. 8. The influence of different types of scattering paths upon the calculated UO_2F_2 XANES, using overlapped muffin-tin spheres. (a) Solid—experiment (shifted −22 eV); short dash—full calc.; long dash—unscreened full calc. (shifted +4 eV); (b) reduced path set; (c) MS one shell; (d) MS one shell, without longer MS paths; (e) SS one shell. The screened final state reproduces the experimental white-line intensity much better than the unscreened final state. Shoulder *A* arises mainly from multiple scattering within the first shell, i.e., the axial oxygens of the uranyl group.

IV. DISCUSSION

The overall success of FEFF6 in the modeling of uranium L_3-edge XANES indicates that its combination of fully relativistic, semirelativistic, and nonrelativistic approximations is adequate for high-Z atoms. Using a somewhat similar treatment of relativistic effects, Guo *et al.* were successful in the modeling of uranium M-edge XANES.[9] The calculated spectra presented here tend to have narrower fine structures, as compared to the experimental spectra. The observed differences are too large to arise solely from an underestimation of instrumental broadening. This disagreement is most likely a consequence of thermal broadening, which was ignored in most of the calculations. When the correlated Debye model was used to model thermal effects for UO_2, the calculations yielded a closer match to experimental linewidths.

Agreement with experiment was generally better when a screened final state was used in FEFF6. One notable exception is for UO_2, where the unscreened final state gave a better prediction of the white-line intensity. This may be a result of a localized final state for the white line, in UO_2. Such localization of the excited electron would effectively screen the core hole, and prevent an external electron from occupying a screening state. Note that the screened final state models shoulder B of the UO_2 XANES better than the unscreened state [see Figs. 1 and 4(a)], suggesting that the shoulder state is not as localized as the white-line state. Experimental evidence of localization for the white line state in UO_2 is clearly seen in Table II; UO_2 has the largest intensity and by far the smallest linewidth of all the white-line experimental data. Based on the UO_2 results, the success of the screened final state in modeling the white-line intensities for most of the uranium intermetallics can be interpreted in terms of a delocalized white-line state. In fact, experimental XANES studies of actinide and rare-earth compounds have been motivated in part by the need to measure the degree of localization of conduction-band electrons. The present results suggest that, with refinement, FEFF calculations may facilitate this measurement. Work is in progress to improve the treatment of multielectron effects, including screening.

The scattering path analysis presented in Sec. III C demonstrated striking differences between UO_2 and the uranium intermetallics. The UO_2 XANES clearly includes contributions from higher-order scattering and from more distant coordination shells, while XANES for most of the intermetallics can be modeled using only single scattering within a small cluster. This contrast may be understood on the basis of crystal symmetry and density. UO_2 possesses the fluorite crystal structure, which has very high symmetry and close packing of atoms in comparison to the other uranium compounds studied. For example, UO_2 has the second-largest atom number density and uranium number density of all the compounds studied here (see Table I). The short interatomic distances and tight packing occur in combination with large degeneracies for the coordination shells around the uranium atoms. Of particular importance is the combination of a fairly short distance to the first uranium coordination shell (3.87 Å) with a large coordination number (12), and similar combinations for the successive uranium shells. A large atomic density will tend to accentuate multiple scattering (MS), simply because there are more paths possible within a given path length. High symmetries also favor MS because multilegged paths have degeneracies related to a product of coordination numbers. Electron-scattering amplitudes increase with atomic number, so the coordination numbers and interatomic distances to uranium atoms are of special importance. The notable first- and second-order scattering contributions of the sixth coordination shell which were demonstrated for UO_2 are easily understood considering that the sixth shell consists of 24 uranium atoms.

The need for a six-shell cluster to model the L_3 XANES of UO_2 is perhaps surprising in light of the successful two-shell modeling of the UO_2 M_3 XANES presented by Guo *et al.*[9] However, sixth-shell contributions found here for the L_3 XANES were specifically identified by modeling an experimental feature (peak D of Fig. 4) $\approx$55 eV above the white-line maximum. Although it is otherwise quite similar, the experimental M_3 spectrum apparently does not exhibit an analogous structure,[9] and thus should not require the six-shell model. This discrepancy between L_3 and M_3 probably results from a difference in core-hole natural linewidths, which were calculated to be 7.4 and $\approx$12 eV for $2p_{3/2}$ and $3p_{3/2}$, respectively.[35,43] The shorter lifetime of the $3p_{3/2}$ core hole should suppress contributions from more distant scatterers. Note, however, that a comparison of UO_2 experimental XANES suggested that the M_3 linewidth is closer to L_3 than the calculated values indicate.[13]

The uranium intermetallics have generally lower-symmetry crystal structures and more open atomic packing, as compared to UO_2. This explains the lack of significant contributions from higher-order scattering and more distant shells for most of the intermetallics. The exceptions are the calculations for UAl_2 and UMn_2, which required the inclusion of six coordination shells to give the best agreement with experiment, and showed some differences when MS was included. These exceptions may result from the relatively large atom number and uranium number densities for these compounds (see Table I), and the large coordination number (12) for the second and third coordination shells of uranium, as compared to the other intermetallics. The MS contribution was shown to arise almost entirely from one path, which gains importance because of a linear arrangement of atoms arising in this crystal structure.

α-U has a rather low-symmetry crystal structure, with five coordination shells within 4 Å. However, it also has a very large density of uranium atoms (see Table I). The latter characteristic may explain the observed influence of MS and fairly distant scatterers in the converged calculation.

The agreement between experiment and calculations was greatly improved for UO_2F_2 by the use of overlapped

muffin-tin spheres in the construction of the scattering potential. The uranyl moiety has, by far, the strongest directional bonding of all the compounds considered here. Nonoverlapped muffin-tin spheres may produce unphysical discontinuities at the edge of the spheres for systems with short bonds, so the need for overlap is expected in UO_2F_2. As a test, calculations using overlapping muffin-tin spheres were also performed for several other uranium compounds. Compared to the nonoverlapped results, these gave either no difference or slightly poorer agreement with experiment. The UO_2F_2 calculation which used overlapped spheres and an unscreened final state predicts a very weak white line [Fig. 8(a)]. Considering the fairly narrow white line observed experimentally, this result is somewhat surprising, especially in light of the discussion for UO_2 above.

The uranium L_3-edge XANES of uranyl compounds consistently exhibit a resonance ≈ 15 eV above the white-line maximum, e.g., shoulder A in Fig. 8. This feature shows only a limited sensitivity to environment, with a similar appearance in aqueous uranyl complexes[22] and in a variety of uranyl solids.[13,14,21] The common factors between all these systems are the uranyl moiety, i.e., a short linear O-U-O group, and the formal +6 oxidation state of uranium. There have been two proposed explanations for this resonance. Based on similarities to the Ce L_3-edge XANES in CeO_2 and CeF_4, the resonance has been attributed to a shake-up process.[27] In this case, the dominant white line and the high-energy shoulder correspond to different electron configurations for the final state. This is inherently a multielectron process and would not be modeled by FEFF6. Evidence for this explanation can be found in the pressure dependence of UO_3 XANES,[27] and in the differences between calculated energies for several core-excited configurations of α-U.[44] The other proposed explanation is that the shoulder is a multiple-scattering resonance associated with the axial U—O bonds.[13,14] This view is supported by the striking polarization dependence of the resonance—it is intense when the linear polarization of the x rays is parallel to the uranyl axis, and nearly absent for the perpendicular case.[45] Until now, neither proposed explanation has been directly tested by theoretical calculations. The present results, shown in Fig. 8, clearly demonstrate a localized multiple-scattering origin for this resonance. However, the possibility of additional contributions to the XANES from multielectron excitations cannot be excluded, in light of the limited agreement between the FEFF calculations and experiment. Contributions to the experimental spectrum from s-symmetry final states, which are ignored by FEFF, might also explain these differences. Further work, both experimental and theoretical, is currently in progress to better characterize the uranyl XANES.

ACKNOWLEDGMENTS

The authors thank G. Kaindl and J. Lawrence for allowing the reproduction of previously published spectra. J. Lawrence is acknowledged for sharing unpublished spectra. S. Zabinsky provided valuable advice in the use of the FEFF6 code. This work was supported in part by the Division of Materials Science, Office of Basic Energy Science, and performed under the auspices of the U.S. Department of Energy by Lawrence Livermore National Laboratory under Contract No. W-7405-ENG-48. Work was also supported in part by the Director, Office of Energy Research, Office of Basic Energy Sciences, Chemical Sciences Division of the U.S. Department of Energy under Contract No. DE-AC03-76SF00098. Experimental measurements were made at SSRL, which is operated by the U.S. Department of Energy, Office of Basic Energy Sciences, Divisions of Chemical Sciences and Materials Science.

[1] *EXAFS and Near Edge Structure,* edited by A. Bianconi, L. Incoccia, and S. Stipcich, Springer Series in Chemical Physics Vol. 27 (Springer-Verlag, Berlin, 1983).

[2] *X-Ray Absorption: Principles, Applications, Techniques of EXAFS, SEXAFS, and XANES,* edited by D. C. Koningsberger and R. Prins (Wiley, New York, 1988).

[3] P. A. Lee, P. H. Citrin, P. Eisenberger, and B. M. Kincaid, Rev. Mod. Phys. **53**, 769 (1981).

[4] L. Fonda, J. Phys. Condens. Matter **4**, 8269 (1992).

[5] J. J. Rehr, R. C. Albers, and S. I. Zabinsky, Phys. Rev. Lett. **69**, 3397 (1992).

[6] R. Gunella, M. Benfatto, A. Marcelli, and C. R. Natoli, Solid State Commun. **76**, 109 (1990).

[7] S.-H. Chou, J. J. Rehr, E. A. Stern, and E. R. Davidson, Phys. Rev. B **35**, 2604 (1987).

[8] T. A. Tyson, Phys. Rev. B **49**, 12 578 (1994).

[9] J. Guo, D. E. Ellis, E. Alp, L. Soderholm, and G. K. Shenoy, Phys. Rev. B **39**, 6125 (1989).

[10] Y. Gao, T. Tiedje, P. C. Wong, and K. A. R. Mitchell, Phys. Rev. B **48**, 15 578 (1993).

[11] E. A. Stern, Phys. Rev. Lett. **49**, 1353 (1982).

[12] M. R. Norman and D. D. Koelling, in *Handbook on the Physics and Chemistry of Rare Earths,* edited by K. A. Gschneidner, Jr., L. Eyring, G. H. Lander, and G. R. Choppin (Elsevier, 1993), Vol. 17.

[13] G. Kalkowski, G. Kaindl, W. D. Brewer, and W. Krone, Phys. Rev. B **35**, 2667 (1987).

[14] J. Petiau, G. Calas, D. Petitmaire, A. Bianconi, M. Benfatto, and A. Marcelli, Phys. Rev. B **34**, 7350 (1986).

[15] J. M. Lawrence, M. L. den Boer, R. D. Parks, and J. L. Smith, Phys. Rev. B **29**, 568 (1984).

[16] G. Kalkowski, G. Kaindl, S. Bertram, G. Schmeister, J. Rebizant, J. C. Spirlet, and O. Vogt, Solid State Commun. **64**, 193 (1987).

[17] P. G. Allen, J. J. Bucher, D. L. Clark, N. M. Edelstein, S. A. Ekberg, J. W. Gohdes, E. A. Hudson, N. Kaltsoyannis, W. W. Lukens, M. P. Neu, P. D. Palmer, T. Reich, D. K. Shuh, C. D. Tait, and B. D. Zwick, Inorg. Chem. (to be published).

[18] D. K. Veirs, C. A. Smith, J. M. Berg, B. D. Zwick, S. F. Marsh, P. Allen, and S. D. Conradson, J. Alloys Compounds **213/214**, 328 (1994).

[19] P. Charpin, A. Dejean, G. Folcher, P. Rigny, and P. Navaza,

J. Chim. Phys. **82**, 925 (1985).
[20]J.-M. Combes, C. Chisholm-Brause, G. E. Brown, Jr., G. A. Parks, S. D. Conradson, P. G. Eller, I. R. Triay, D. E. Hobart, and A. Meijer, Environ. Sci. Technol. **26**, 376 (1992).
[21]F. Farges, R. C. Ewing, and G. E. Brown, Jr., J. Mater. Res. **8**, 1983 (1993).
[22]C. Chisholm-Brause, S. D. Conradson, C. T. Buscher, P. G. Eller, and D. E. Morris, Geochim. Cosmochim. Acta **58**, 3625 (1994).
[23]T. D. Waite, J. A. Davis, T. E. Payne, G. A. Waychunas, and N. Xu, Geochim. Cosmochim. Acta **58**, 5465 (1994).
[24]S. I. Zabinsky, J. J. Rehr, A. Ankudinov, R. C. Albers, and M. J. Eller, Phys. Rev. B **52**, 2995 (1995).
[25]J. J. Rehr, J. Mustre de Leon, S. I. Zabinsky, and R. C. Albers, J. Am. Chem. Soc. **113**, 5135 (1991).
[26]J. Mustre de Leon, J. J. Rehr, S. I. Zabinsky, and R. C. Albers, Phys. Rev. B **44**, 4146 (1991).
[27]S. Bertram, G. Kaindl, J. Jové, M. Pagès, and J. Gal, Phys. Rev. Lett. **63**, 2680 (1989).
[28]S. I. Zabinsky, Ph.D. thesis, University of Washington, 1993.
[29]E. Hudson, E. Moler, Y. Zheng, S. Kellar, P. Heimann, Z. Hussein, and D. A. Shirley, Phys. Rev. B **49**, 3701 (1994).
[30]M. Newville, P. Livins, Y. Yacoby, J. J. Rehr, and E. A. Stern, Phys. Rev. B **47**, 14 126 (1993).
[31]J. J. Rehr, C. H. Booth, F. Bridges, and S. I. Zabinsky, Phys. Rev. B **49**, 12 347 (1994).
[32]T. A. Tyson, K. O. Hodgson, C. R. Natoli, and M. Benfatto, Phys. Rev. B **46**, 5997 (1992).
[33]J. Desclaux, J. Phys. B **4**, 631 (1971); Comput. Phys. Commun. **9**, 31 (1975).
[34]T. L. Loucks, *Augmented Plane Wave Method* (Benjamin, New York, 1967).
[35]M. O. Krause and J. H. Oliver, J. Phys. Chem. Ref. Data **8**, 329 (1979).
[36]B. T. M. Willis, Proc. R. Soc. London Ser. A **274** (1963).
[37]E. Sevillano, H. Meuth, and J. J. Rehr, Phys. Rev. B **20**, 4908 (1979).
[38]B. W. Veal and A. P. Paulikas, Phys. Rev. B **31**, 5399 (1985).
[39]S.-J. Oh. G.-H. Gweon, and J.-G. Park, Phys. Rev. Lett. **68**, 2850 (1992).
[40]K. Hermann and P. S. Bagus, Phys. Rev. B **28**, 560 (1983).
[41]E. Umbach, Surf. Sci. **117**, 482 (1982).
[42]J. Lawrence (private communication).
[43]J. F. Herbst and J. W. Wilkins, Phys. Rev. B **38**, 1027 (1988).
[44]S. I. Salem, S. L. Panossian, and R. A. Krause, At. Data Nucl. Data Tables **14**, 91 (1974).
[45]D. H. Templeton and L. K. Templeton, Acta Crystallogr. Sec. A **38**, 62 (1982).
[46]R. W. G. Wyckoff, *Crystal Structures,* 2nd ed. (Interscience, New York, 1963), Vol. 1.
[47]R. W. G. Wyckoff, *Crystal Structures,* 2nd ed. (Interscience, New York, 1964), Vol. 2.
[48]M. Atoji and M. J. McDermott, Acta Crystallogr. Sec. B **26**, 1540 (1970).
[49]N. C. Baenziger, R. E. Rundle, A. I. Snow, and A. S. Wilson, Acta Crystallogr. **3**, 34 (1950).
[50]W. B. Pearson, *Handbook of Lattice Spacing and Structures of Metals and Alloys* (Pergamon, New York, 1967), Vol. 2.